Data supplement for Norman et al., A developmental study of resting-state connectivity and response to psychostimulant treatment in ADHD. Am J Psychiatry (doi: 10.1176/appi.ajp.2021.20091342)

SUPPLEMENTARY METHODS

fMRI Acquisition and Preprocessing

Resting-state fMRI was acquired using a gradient-echo-planar series [repetition time = 2,500 ms; echo time = 27 ms; flip angle = 90°; 44 axial contiguous interleaved slices per volume; 2.8-mm slice thickness; field of view = 22 cm; 64 × 64 acquisition matrix; single-voxel volume = 3.4 mm, 3.4 mm, 2.8 mm] with whole-brain coverage on a 3-T scanner for 315 s (General Electric). Subjects were instructed to lie in the scanner at rest, looking at a fixation cross. A baseline-weighted anatomical image [magnetization prepared rapid acquisition gradient recalled echo sequence (MP RAGE): 124 axial slices, 1.3-mm slice thickness, field of view = 22 cm, 224 × 224 acquisition matrix] was acquired to assist with the alignment of the functional image with normalization to stereotaxic space. Participants were scanned in the afternoon or early evening.

Preprocessing of fMRI images

Data were preprocessed using fMRIPrep version 1.3.2, a Nipype based tool (1, 2). Each T1w (T1-weighted) volume was corrected for intensity non-uniformity using N4BiasFieldCorrection v2.1.0 (3) and skull-stripped using antsBrainExtraction.sh v2.1.0 (using the OASIS template). Spatial normalization to MNI space was performed through nonlinear

registration with the antsRegistration tool of ANTs v2.1.0 (4), using brain-extracted versions of both T1w volume and template. Brain tissue segmentation of cerebrospinal fluid (CSF), white-matter (WM) and gray-matter (GM) was performed on the brain-extracted T1w using fast (FSL v5.0.9) (5).

Functional data were slice time corrected using 3dTshift from AFNI v16.2.07 (6) and motion corrected using mcflirt (FSL v5.0.9) (7). This was followed by co-registration to the corresponding T1w using boundary-based registration (8) with six degrees of freedom, using flirt (FSL). Motion correcting transformations, BOLD-to-T1w transformation and T1w-to-template (MNI) warp were concatenated and applied in a single step using antsApplyTransforms (ANTs v2.1.0) using Lanczos interpolation.

The final rsFMRI preprocessing steps used the xcpengine toolbox version 1.0 (https://xcpengine.readthedocs.io), and the 36-parameter + despiking functional design for deconvolution (9–13). Despiking refers to the removal of and interpolation over intensity outliers in each voxel's time series using AFNI's 3DDESPIKE utility (6). We then performed demeaning and removal of any linear or quadratic trends. The 36-parameters regressed from the timeseries included the 6 motion estimates, global signal, and white matter and cerebrospinal fluid-derived time series), and then their derivatives, quadratic terms, and squares of derivatives (9, 10). Temporal filtering was performed using a bandpass filter of 0.01–0.08 Hz (first-order Butterworth filter (14)) and images were smoothed in SUSAN using a Gaussian-weighted kernel with 6 mm FWHM (15).

All raw images underwent visual inspection. Quality control procedures also involved inspecting visual reports produced by fMRIPrep for brain extraction, segmentation, EPI to T1 co-

registration, co-registration to standard space and the placement of white matter and cerebrospinal masks. Carpet plots summarizing the time series for all voxels within the brain mask were also checked (16). Only scans with a mean relative root-mean-square displacement (mean-RMS) ≤0.75 were included in this analysis, based on similar thresholds used previously in ADHD research (17–19).

Excluded Scans

All potential scans were collected at least six months apart, and we included up to 5 timepoints per subject.

There was a total of 270 completed resting-state scans collected from 132 medicated patients with coinciding treatment response and medication dosage information. For three scans, no T1 images were available. Sixty-eight scans were removed due to excessive motion. One scan was removed due to very poor coverage and excessive motion. Two scans failed to complete the preprocessing stream successfully. This left a total of 196 usable scans from 110 patients.

There were an initial 388 potentially includable scans available for typically developing controls. From these, one did not have a corresponding T1 image. Six were excluded due to failing to complete the preprocessing stream (e.g., due to poor coregistration or poor segmentation). A further 51 scans were removed due to excessive motion. This meant that the final sample included 330 scans from 142 subjects.

Functional Network Definitions

Our chosen networks and regions of interest (ROIs) were based on the existing literature (20–23). Specifically, the cingulo-opercular network was included based on its close association

with ADHD, particularly via task-based fMRI studies (21). Meta-analyses and literature reviews point to hypoactivation within this network to be the most common functional neuroimaging finding in the disorder (20, 24), which furthermore normalizes with psychostimulant treatment (20). Striato-thalamic regions were chosen based on their importance within the dopaminergic system, as well as due to previously reported findings of altered striato-thalamic gray matter volume, activation and connectivity in patients with ADHD relative to controls (20, 24–26). Finally, influential theoretical models of ADHD suggest that symptoms may, in part, be attributable to default mode dysfunction, which has also been reported to normalize with psychostimulant treatments (23, 27, 28).

Regions of interest for the cingulo-opercular network (sometimes referred to in the literature as the salience network) included frontal operculum, insula, dorsal anterior cingulate cortex and posterior medial frontal cortex (29–31). Regions included in the default mode network were precuneus, posterior cingulate cortex, angular gyrus, middle temporal lobe and anterior medial prefrontal cortex (29, 32). Cingulo-opercular and default-mode network regions of interest were extracted from the Harvard-Oxford atlas by placing a 5-mm spherical radius around the (approximate) center of each region as given by FMRIB Software Library's (FSL) View software (www.fmrib.ox.ac.uk/fsl/fslview) (33). Striato-thalamic regions of interest were based on coordinates provided by Di Martino et al (striatum) and Welsh et al (thalamus) (34, 35), and included dorsal caudate, dorsal putamen, dorsomedial thalamus, ventral putamen and nucleus accumbens (24, 29, 34–36). Coordinates and corresponding Harvard-Oxford labels are provided in Table S1. See Figure S1.

Edgewise Analyses

In addition to performing analyses at the network level, we also performed exploratory edge-level analyses. This involved performing the same statistical procedures as applied at the network level on each of the 253 individual ROI-to-ROI connections (e.g., dACC to right insula; PCC to right thalamus), and correcting for the number of connections using the Benjamini-Hochberg method (37). See Table S3 below.

Statistical Analysis

Clinical and demographic analyses

Gender composition was compared between patients and typically developing controls using the chi-square test. Independent t-tests were used to compare age, symptoms and motion between patients and typically developing controls at each timepoint. Other analyses were performed using linear mixed models within the nlme package (38) for R (http://www.r-project.org).

To examine the relationship between treatment response (% symptom reduction when rated on versus off medication) and age, sex, dosage (daily methylphenidate-equivalent mg/kg), off-medication symptoms and psychostimulant class (methylphenidate versus amphetamine) the following model was used:

$$\text{Treatment response}_{ij}=\text{intercept}+d_{ij}+B_1(\text{age}_{ij})+B_2(\text{sex}_i)+B_3(\text{dosage}_{ij})+B_4(\text{symptoms}_{ij})+B_5(\text{psychostimulant class}_{ij})+e_{ij}$$

where d_{ij} are nested random effects modeling within-person and within family dependence, the intercept and B terms are fixed effects, and e_{ij} represents the residual error. The i subscript denotes subject, the j subscript denotes time point.

To examine the relationship between off medication symptoms and age, while controlling for sex, the following model was used.

$$Symptoms_{ij}=intercept+d_{ij}+\mathbf{B_1(age_{ij})}+B_2(sex_i)+e_{ij}$$

To examine the relationship between dosage and age, psychostimulant type and off-medications symptoms while controlling for sex the following model was used.

$$Dosage_{ij}=intercept+d_{ij}+B_1(age_{ij})+B_2(sex_i)+B_3(psychostimulant\ class_{ij})+ B_4(symptoms_{ij})e_{ij}$$

To examine the association between mean-RMS and treatment response, we ran the following model.

$$Mean\text{-}RMS_{ij} =intercept+d_{ij}+B_1(age_{ij})+B_2(sex_i)+\mathbf{B_3(treatment\ response_{ij})}+e_{ij}$$

Brain analyses

Model 1

In model 1 we examined the interaction between treatment response (% symptom reduction while on as compared with off psychostimulant medication) and age while controlling for the main effects of age, sex, dosage, off-medication symptoms, treatment response and motion. The model was as follows.

$$Connectivity_{ij}=intercept+d_{ij}+B_1(age_{ij})+B_2(sex_i)+B_3(dosage_{ij})+B_4(symptoms_{ij})+B_5(treatment\ response_{ij})+B_6(motion_{ij})+\mathbf{B_7(age_{ij}*treatment\ response_{ij})}+e_{ij},$$

where d_{ij} are nested random effects modeling within person and within family dependence, the intercept and B terms are fixed effects, and e_{ij} represents the residual error. The i subscript denotes subject, the j subscript denotes timepoint. The interaction of interest is in **bold**.

Model 2

In model 2 we compared connectivity changes with age between "better" treatment responses (> mean symptom reduction), "worse" treatment responses (< mean symptom reduction) and typically developing controls for network metrics significant in model 1 (i.e., within-network cingulo-opercular connectivity). In model 2 we thus regressed connectivity metrics against the interaction between treatment response group (better responses, worse responses, typically developing controls) and age while controlling for the main effects of age, sex, motion and treatment response group. Model 2 was therefore as follows.

$Connectivity_{ij}$ =intercept+d_{ij}+$B_1(age_{ij})$+$B_2(sex_i)$+$B_3(motion_{ij})$+B_4(treatment response $group_{ij}$)+$\mathbf{B_5(age_{ij}*treatment\ response\ group_{ij})}$+$e_{ij}$, where group was a three-level unordered factor (better responses, worse responses, typically developing controls).

For this model, we first examined the F-test for the interaction between group and age using the *anova.lme* function in nlme. To probe significant findings, we also examined pairwise comparisons for differences in the relationships between age and connectivity (i.e. better versus worse responses, better responses versus typically developing controls, worse responses versus typically developing controls) using the *summary.lme* function.

Model 3

To further understand the relationships between age and connectivity for each treatment response group, we performed the following model at each level of group (i.e. separately for better responses, worse responses and typically developing controls).

$$Connectivity_{ij}=intercept+d_{ij}+\mathbf{B_1(age_{ij})}+B_2(motion_{ij})+ B_3(Sex_i)e_{ij}$$

Main effects of treatment response

In addition to examining treatment response by age interactions, we also examined for the main effect of treatment response on brain connectivity for each of the networks while controlling for age, sex, dosage, motion, and off-medication symptoms. This was performed using the model below:

$$Connectivity_{ij}=intercept+d_{ij}+B_1(age_{ij})+B_2(sex_i)+B_3(dosage_{ij})+B_4(symptoms_{ij})+B_5(motion_{ij})+\mathbf{B_6(treatment\ response_{ij})}+e_{ij}$$

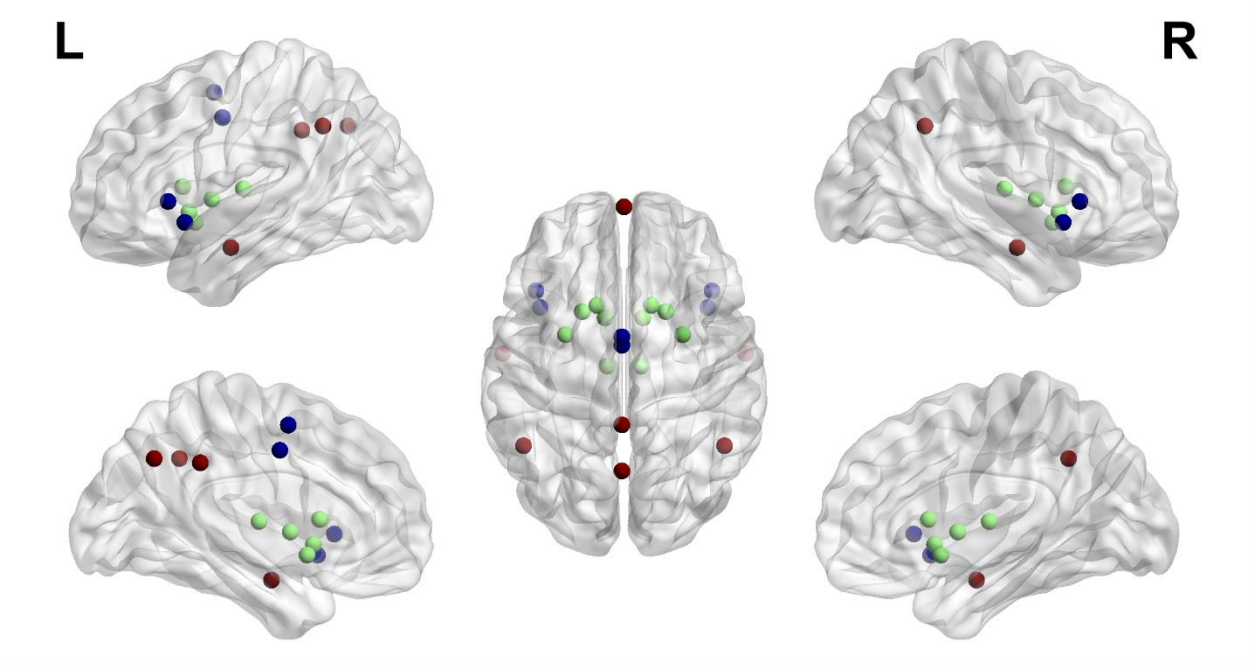

FIGURE S1. Regions of interest from the three networks of interest. Blue=Cingulo-opercular network, green=Striato-thalamic network, red=Default-mode network. Corresponding region labels and coordinates are provided in Table S1.

TABLE S1. Region labels and coordinates for cingulo-opercular, striato-thalamic and default mode network regions of interest

Region	Harvard-Oxford label	MNI x,y,z	Network
Insula	Insular cortex	+/-40,14,-8	Cingulo-opercular
Frontal operculum	Frontal operculum cortex	+/-42,22,2	Cingulo-opercular
Dorsal anterior cingulate cortex	Cingulate gyrus, anterior division	0,-4,42	Cingulo-opercular
Posterior medial frontal cortex	Juxtapositional lobule cortex (formerly supplementary motor cortex)	0,0,54	Cingulo-opercular
Precuneus	Precuneous cortex	0,-64,38	Default mode
Posterior cingulate cortex	Cingulate gyrus, posterior division	0,-42,36	Default mode
Middle temporal lobe	Middle temporal gyrus, posterior division	+/-58,-8,-20	Default mode
Angular gyrus	Angular gyrus	+/-48,-52,38	Default mode
Anterior medial prefrontal cortex	Frontal pole	0,62,-2	Default mode
Dorsal caudate	--	+/-13,15,9	Striato-thalamic
Dorsal putamen	--	+/-28,1,3	Striato-thalamic
Dorsomedial thalamus	--	+/-8,-14,8	Striato-thalamic
Ventral putamen	--	+/-20,12,-3	Striato-thalamic
Nucleus accumbens	--	+/-9,9,-8	Striato-thalamic

Abbreviations: MNI, Montreal Neurological Institute.

SUPPLEMENTARY RESULTS

Symptom Subtypes

The majority (N=75; 68.18%) of patients with ADHD met criteria for the combined subtype, while N=31 (28.18%) met criteria for the predominantly inattentive subtype and four patients (3.64%) met criteria for the predominantly hyperactive/impulsive subtype.

Sensitivity Analyses and Robustness Checks

A small number of patients were taking non-stimulant medications including guanfacine (n=8) and atomoxetine (n=1) for ADHD symptoms. The interaction between treatment response and age on cingulo-opercular connectivity remained unchanged after removing timepoints where subjects were taking additional medications (*B*=-0.07, t=-3.29, p=0.002, 95%CI=-0.1, -0.03). With regards to comorbidities, we considered anxiety, except specific phobias (N=5 with generalized anxiety disorder), oppositional defiance disorder (N=14) as well as community diagnosed autism spectrum disorders (N=2). No patients met criteria for mood disorders at any included timepoint of the study. The interaction again remained significant after removing patient scans associated with comorbid diagnoses (*B*=-0.06, t=-3.2, p=0.002, 95%CI=-0.1,-0.02). Symptom reduction was not associated with mean-RMS (*B*=-0.07, t=-1.4, p=0.16, 95%CI=-0.2, 0.03), which also did not differ between patients and controls (p>0.1; see Table S2). Moreover, the interaction remained after adopting a stricter motion exclusion criterion (mean-RMS>0.35; *B*=-0.07, t=-3.4, p=0.001, 95%CI=-0.1, -0.03). The interaction remained significant when restricted to the first two (*B*=-0.06, t=-2.56, p=0.01, 95%CI=-0.1, -0.01) and first three (*B*=-0.06, t=-3.1, p=0.003, 95%CI=-0.1, -0.02) scans. In addition, the finding remained when examining inattention (*B*=-0.05, t=-3.1, p=0.003, 95%CI=-0.09, -0.02) and hyperactivity/impulsivity (*B*=-

0.04, t=-2.47, p=0.02, 95%CI=-0.08, -0.008) symptoms separately. Finally, the finding remained unchanged when controlling for psychostimulant class (*B*=0.07, t=-3.55, p=0.0007, 95% CI=-0.1, -0.03), and adding an additional interaction term for age by treatment response by psychostimulant class to the model decreased model fit, as determined by the Bayesian information criterion (without additional interaction term, -35.23; including additional interaction term, -1.1). Moreover, this interaction was nonsignificant (*B*=-0.03, t=-0.82, p=0.4, 95% CI=-0.05, 0.1).

Post Hoc Power

The age by treatment response interaction term was associated with medium (d=0.51) to large (d=0.79) effect sizes, depending on how the degrees of freedom were estimated, with medium effects arising from the more conservative Satterthwaite estimate of degrees of freedom for mixed models run in lmertest (39), and the latter using the default degrees of freedom provided by the nlme package (40). Post-hoc calculations performed using the SimR and nlmeU packages showed our sample size was powered at >0.8 to detect these medium and large effect sizes with an alpha of α=0.05 and α=0.01 (41, 42). The α=0.01 threshold was included as an approximate estimation of the required alpha accounting for the FDR correction for the three networks. These calculations should be interpreted with caution as they are post-hoc (43) and did not inform the initial study design.

TABLE S2. Mean RMS at each timepoint for patients with ADHD and typically developing controls

	ADHD		TD		Statistical test
	Mean	**SD**	**Mean**	**SD**	
Time 1	0.29	0.18	0.26	0.18	t(250)=1.3, p=0.19
Time 2	0.24	0.17	0.21	0.16	t(139)=1.06, p=0.29
Time 3	0.19	0.13	0.17	0.13	t(70)=0.57, p=0.57
Time 4	0.17	0.18	0.16	0.13	t(40)=0.19, p=0.85
Time 5	0.11	0.04	0.15	0.09	t(17)=0.85, p=0.41

Abbreviations: ADHD, attention-deficit/hyperactivity disorder; TD, typically developing.

TABLE S3. Edgewise (ROI-to-ROI) connections that were significant (p<0.05) before correction for multiple comparisons

ROI 1	ROI 2	Network(s)	*B*	SE	t	Uncorrected p	FDR Corrected p
R insula	R frontal operculum	Cingulo-opercular	-0.09	0.03	-2.92	0.004	0.6
L insula	R insula	Cingulo-opercular	-0.09	0.03	-2.81	0.006	0.6
R insula	dACC	Cingulo-opercular	-0.08	0.03	-2.64	0.01	0.6
R caudate	R angular gyrus	Striato-thalamic/DMN	-0.07	0.03	-2.64	0.01	0.6
R frontal operculum	R ventral striatum	Cingulo-opercular/ striato-thalamic	-0.07	0.03	-2.34	0.03	0.8
R insula	L caudate	Cingulo-opercular/ striato-thalamic	-0.07	0.03	-2.31	0.04	0.8
L ventral putamen	L angular gyrus	Striato-thalamic/DMN	-0.06	0.03	-2.24	0.04	0.8
R insula	R angular gyrus	Cingulo-opercular /DMN	-0.06	0.03	-2.14	0.04	0.8
dACC	L caudate	Cingulo-opercular/ striato-thalamic	-0.06	0.03	-2.09	0.03	0.8
R insula	pMFC	Cingulo-opercular	-0.06	0.03	-2.08	0.03	0.8
L insula	dACC	Cingulo-opercular	-0.07	0.03	-2.03	<0.05	0.8
L insula	pMFC	Cingulo-opercular	-0.06	0.03	-2.01	<0.05	0.8

Abbreviations: dACC, dorsal anterior cingulate cortex; DMN, default mode network; FDR, false discovery rate; L, left; pMFC, posterior medial frontal cortex; R, right; SE, standard error.

SUPPLEMENTARY REFERENCES

1. Esteban O, Markiewicz CJ, Blair RW, et al.: fMRIPrep: a robust preprocessing pipeline for functional MRI. Nature methods 2019; 16:111–116

2. Gorgolewski K, Burns CD, Madison C, et al.: Nipype: a flexible, lightweight and extensible neuroimaging data processing framework in python. Frontiers in neuroinformatics 2011; 5:13

3. Tustison NJ, Avants BB, Cook PA, et al.: N4ITK: improved N3 bias correction. IEEE transactions on medical imaging 2010; 29:1310–1320

4. Avants BB, Epstein CL, Grossman M, et al.: Symmetric diffeomorphic image registration with cross-correlation: evaluating automated labeling of elderly and neurodegenerative brain. Med Image Anal 2008; 12:26–41

5. Zhang Y, Brady M, Smith S: Segmentation of brain MR images through a hidden Markov random field model and the expectation-maximization algorithm. IEEE transactions on medical imaging 2001; 20:45–57

6. Cox RW: AFNI: software for analysis and visualization of functional magnetic resonance neuroimages. Computers and Biomedical research 1996; 29:162–173

7. Jenkinson M, Bannister P, Brady M, et al.: Improved optimization for the robust and accurate linear registration and motion correction of brain images. Neuroimage 2002; 17:825–841

8. Greve DN, Fischl B: Accurate and robust brain image alignment using boundary-based registration. Neuroimage 2009; 48:63–72

9. Ciric R, Wolf DH, Power JD, et al.: Benchmarking of participant-level confound regression strategies for the control of motion artifact in studies of functional connectivity. Neuroimage 2017; 154:174–187

10. Ciric R, Rosen AFG, Erus G, et al.: Mitigating head motion artifact in functional connectivity MRI. Nat Protoc 2018; 13:2801–2826

11. Gur RE, Moore TM, Rosen AFG, et al.: Burden of Environmental Adversity Associated With Psychopathology, Maturation, and Brain Behavior Parameters in Youths. JAMA Psychiatry 2019; 76:966–975

12. Cui Z, Li H, Xia CH, et al.: Individual variation in functional topography of association networks in youth. Neuron 2020;

13. Gu S, Xia CH, Ciric R, et al.: Unifying the Notions of Modularity and Core–Periphery Structure in Functional Brain Networks during Youth. Cerebral Cortex 2020; 30:1087–1102

14. Hallquist MN, Hwang K, Luna B: The nuisance of nuisance regression: spectral misspecification in a common approach to resting-state fMRI preprocessing reintroduces noise and obscures functional connectivity. Neuroimage 2013; 82:208–225

15. Smith SM, Brady JM: SUSAN—a new approach to low level image processing. International journal of computer vision 1997; 23:45–78

16. Power JD: A simple but useful way to assess fMRI scan qualities. Neuroimage 2017; 154:150–158

17. Francx W, Oldehinkel M, Oosterlaan J, et al.: The executive control network and symptomatic improvement in attention-deficit/hyperactivity disorder. Cortex 2015; 73:62–72

18. Pruim RHR, Beckmann CF, Oldehinkel M, et al.: An Integrated Analysis of Neural Network Correlates of Categorical and Dimensional Models of Attention-Deficit/Hyperactivity Disorder. Biological Psychiatry: Cognitive Neuroscience and Neuroimaging 2019; 4:472–483

19. Von Rhein D, Oldehinkel M, Beckmann CF, et al.: Aberrant local striatal functional connectivity in attention-deficit/hyperactivity disorder. Journal of Child Psychology and Psychiatry 2016; 57:697–705

20. Rubia K: Cognitive neuroscience of attention deficit hyperactivity disorder (ADHD) and its clinical translation. Frontiers in human neuroscience 2018; 12:100

21. Lukito S, Norman L, Carlisi C, et al.: Comparative meta-analyses of brain structural and functional abnormalities during cognitive control in attention-deficit/hyperactivity disorder and autism spectrum disorder. Psychological Medicine 2020; 50:894–919

22. Rubia K, Alegria AA, Cubillo AI, et al.: Effects of stimulants on brain function in attention-deficit/hyperactivity disorder: a systematic review and meta-analysis. Biological psychiatry 2014; 76:616–628

23. Bozhilova NS, Michelini G, Kuntsi J, et al.: Mind wandering perspective on attention-deficit/hyperactivity disorder. Neurosci Biobehav Rev 2018; 92:464–476

24. Lukito S, Norman L, Carlisi C, et al.: Comparative meta-analyses of brain structural and functional abnormalities during cognitive control in attention-deficit/hyperactivity disorder and autism spectrum disorder. Psychol Med 2020; 1–26

25. Stahl SM, Stahl SM: Stahl's essential psychopharmacology: neuroscientific basis and practical applications. Cambridge university press, 2013

26. Faraone SV: The pharmacology of amphetamine and methylphenidate: relevance to the neurobiology of attention-deficit/hyperactivity disorder and other psychiatric comorbidities. Neuroscience & Biobehavioral Reviews 2018; 87:255–270

27. Liddle EB, Hollis C, Batty MJ, et al.: Task-related default mode network modulation and inhibitory control in ADHD: Effects of motivation and methylphenidate. Journal of Child Psychology and Psychiatry 2011; 52:761–771

28. Peterson BS, Potenza MN, Wang Z, et al.: An FMRI study of the effects of psychostimulants on default-mode processing during Stroop task performance in youths with ADHD. American Journal of Psychiatry 2009; 166:1286–1294

29. Power JD, Cohen AL, Nelson SM, et al.: Functional network organization of the human brain. Neuron 2011; 72:665–678

30. Uddin LQ: Salience processing and insular cortical function and dysfunction. Nature reviews neuroscience 2015; 16:55–61

31. Cai W, Griffiths K, Korgaonkar MS, et al.: Inhibition-related modulation of salience and frontoparietal networks predicts cognitive control ability and inattention symptoms in children with ADHD. Molecular Psychiatry 2019; 1–10

32. Yeo BT, Krienen FM, Sepulcre J, et al.: The organization of the human cerebral cortex estimated by intrinsic functional connectivity. Journal of neurophysiology 2011;

33. Smith SM, Jenkinson M, Woolrich MW, et al.: Advances in functional and structural MR image analysis and implementation as FSL. Neuroimage 2004; 23:S208–S219

34. Di Martino A, Scheres A, Margulies DS, et al.: Functional connectivity of human striatum: a resting state FMRI study. Cerebral cortex 2008; 18:2735–2747

35. Welsh RC, Chen AC, Taylor SF: Low-frequency BOLD fluctuations demonstrate altered thalamocortical connectivity in schizophrenia. Schizophrenia bulletin 2010; 36:713–722

36. Fitzgerald KD, Welsh RC, Stern ER, et al.: Developmental alterations of frontal-striatal-thalamic connectivity in obsessive-compulsive disorder. Journal of the American Academy of Child & Adolescent Psychiatry 2011; 50:938-948. e3

37. Benjamini Y, Hochberg Y: Controlling the false discovery rate: a practical and powerful approach to multiple testing. Journal of the Royal statistical society: series B (Methodological) 1995; 57:289–300

38. Pinheiro J, Bates D, DebRoy S, et al.: nlme: Linear and Nonlinear Mixed Effects Models [Internet]. 2020Available from: https://CRAN.R-project.org/package=nlme

39. Kuznetsova A, Brockhoff PB, Christensen RH: lmerTest package: tests in linear mixed effects models. Journal of statistical software 2017; 82:1–26

40. Pinheiro J, Bates D: Mixed-effects models in S and S-PLUS. Springer Science & Business Media, 2006

41. Galecki A, Burzykowski T: Linear Mixed-Effects Models Using R: A Step-by-Step Approach [Internet]. First. New York, Springer, 2013Available from: http://www-personal.umich.edu/ agalecki

42. Green P, MacLeod CJ: SIMR: an R package for power analysis of generalized linear mixed models by simulation. Methods in Ecology and Evolution 2016; 7:493–498

43. Plate JD, Borggreve AS, van Hillegersberg R, et al.: Post hoc power calculation: observing the expected. Annals of surgery 2019; 269:e11